Tracing Quenching in Nearby Galaxies Through Inner Surface Mass Density and Cold Gas Content

EVANGELA E. SHREAD[†], TREVOR J. WEISS[†], JEROME J. FANG, AND CAMERON LAW^{1,4}

¹Department of Astronomy, Orange Coast College, Costa Mesa, CA 92626
 ²Division of Physics, Math and Astronomy, California Institute of Technology, Pasadena, CA 91125
 ³Department of Physics and Astronomy, California State University, Long Beach, Long Beach, CA 90840
 ⁴Department of Physics and Astronomy, University of California, Irvine, Irvine, CA 92697

ABSTRACT

The inner stellar mass surface density within 1 kpc, Σ_1 , has emerged as a suitable proxy for bulge growth and galaxy quenching. However, the dependence of cold gas content on Σ_1 has not been thoroughly explored. In this paper, we examine the relationship between Σ_1 , as well as the mass-relative parameter $\Delta\Sigma_1$, and the atomic $(f_{\rm HI})$ and molecular $(f_{\rm H2})$ cold gas fractions in massive, nearby galaxies. We utilize a sample of 341 galaxies with HI data and 201 galaxies with H₂ data from the xGASS and xCOLDGASS surveys, spanning $0.02 \le z \le 0.05$ and a stellar mass range of $10^{10} \le M_*/M_\odot \le 10^{11.5}$. While we observe that a decline in both $f_{\rm HI}$ and $f_{\rm H2}$ is associated with increasing Σ_1 , we find that $f_{\rm H2}$ shows a sharper decline above a threshold value of $\Delta\Sigma_1 = 0$. In addition, the fraction of galaxies with AGN activity (Seyferts and LINERs) increases with $\Delta\Sigma_1$, with the greatest increase occurring between $0 \lesssim \Delta\Sigma_1 \lesssim 0.2$ dex. We propose an evolutionary track in the plane of $f_{\rm H2} - \Delta\Sigma_1$, whereby molecular gas depletion at fixed mass coincides with a rise in AGN activity. Our results suggest that central bulge growth is more tightly coupled to the depletion of molecular gas rather than atomic gas, with AGN feedback possibly contributing to this process. Our work highlights the utility of Σ_1 and $\Delta\Sigma_1$ as tracers of quenching in massive galaxies.

Keywords: Galaxy Structure (622) — Molecular gas (1073) — Interstellar atomic gas (833)

1. INTRODUCTION

Star formation quenching and the processes that regulate it are integral to understanding galaxy evolution. Two important markers of quenching are variations in galaxy structure and a decline in the availability of cold gas. The relationship between cold gas content and galaxy structure has been studied extensively, beginning with early works which established a connection between Hubble morphological type and global cold gas content. The HI gas fraction $(f_{\rm HI} \equiv M_{\rm HI}/M_*)$ increases along the Hubble sequence from early- to late-type galaxies (e.g. Roberts 1969; Young & Knezek 1989; Sage 1993; Conselice 2014). There exists less variation in the H_2 gas fraction ($f_{\rm H2} \equiv M_{\rm H2}/M_*$) among spiral morphological types, but elliptical types have appreciably lower fractional H₂ mass content and often constitute nondetections in targeted surveys (e.g. Young & Scoville 1991; Sage 1993; Roberts & Haynes 1994; Boselli et al. 2014).

Scaling relations between galactic structure and cold gas mass offer a means of quantifying the interplay between gas content and galaxy evolution. There have been many studies of the relationship between HI and H₂ content and structural parameters, such as stellar mass surface density (e.g. Saintonge et al. 2011; Catinella et al. 2013; Brown et al. 2015; Saintonge et al. 2017; Catinella et al. 2018; Baker et al. 2021); the half-light or effective radius (e.g. Yesuf & Ho 2019; Lin et al. 2020); Sérsic index (e.g. Fisher et al. 2013; Namiki et al. 2021); and non-parametric measures such as concentration index, asymmetry, and the Gini coefficient (e.g. Catinella et al. 2010; Wang et al. 2011; Kauffmann et al. 2012; Zhou et al. 2018; Namiki et al. 2021; Davis et al. 2022).

The strongest cold gas scaling relations with galactic structure typically involve stellar mass and stellar mass surface density, defined in this work as $\mu_* \equiv 0.5 M_*/\pi R_{50,z}^2$, where $R_{50,z}$ is the half-light radius computed from the SDSS z band flux. Stellar mass surface density has been used to quantify the prominence of the central bulge component, whereby galaxies become bulge-dominated at $\log \mu_* > 8.7 M_{\odot} \ \mathrm{kpc}^{-2}$ (Catinella

¹ † Authors contributed equally.

et al. 2010). For nearby galaxies, μ_* is anti-correlated with both $f_{\rm HI}$ and $f_{\rm H2}$, such that more bulge-dominated galaxies have lower gas fractions (e.g. Catinella et al. 2010; Saintonge et al. 2017). Stellar mass is strongly anti-correlated with atomic gas fraction; $f_{\rm HI}$ scales with log M_* with a slope ranging from -0.3 to -0.9 dex, corresponding to a drop of $\sim 70-80\%$ in the gas fraction per dex in M_* (e.g. Brown et al. 2015; Catinella et al. 2018; Hunt et al. 2020). In contrast, molecular gas fraction shows a weak dependence with M_* , with previous studies finding a near-flat relation, e.g. a median of log $f_{\rm H_2} \simeq -0.99 \pm 0.22$ and a slope consistent with zero over a broad mass range (Saintonge et al. 2011, 2017).

The focus of this paper is to examine the relationship between cold gas content and the stellar mass surface density within 1 kpc of the galactic center (Σ_1) in nearby, massive galaxies. While similar to μ_* , Σ_1 measures the stellar mass surface density within a smaller, constant radius. Σ_1 and similar parameters (such as the inner surface mass density within 1.5 or 2 kpc) have become popular metrics in recent years to identify and examine galaxies that have been quenched. Early works presented Σ_1 as a proxy for central bulge growth and for central black hole mass $(M_{\rm BH})$, and have proposed that once galaxies reach a mass-dependent Σ_1 threshold value, their star formation is shut down (Cheung et al. 2012; Fang et al. 2013; Barro et al. 2017). For this reason, Σ_1 is often used as a tracer of galactic evolution from the star-forming to the quiescent phase. As Σ_1 grows at fixed mass, galaxies transition through the green valley from the blue sequence to the red (Fang et al. 2013), and at fixed redshift, galaxies evolve along the star formation main sequence (MS) via inside-out growth, traced by increasing Σ_1 (Barro et al. 2017).

 Σ_1 is tightly correlated with M_* (e.g. Fang et al. 2013). The mass-trend-removed parameter $\Delta\Sigma_1$ is defined relative to the structural valley within the $\Sigma_1 - M_*$ plane. This is a visual feature in the plot which, at fixed mass, appears as a trough between two higher density populations of low and high Σ_1 (Luo et al. 2020). While not exactly the same as the star-formation green valley, Luo et al. (2020) showed that $\Delta\Sigma_1$ as defined in this manner is related to the star-forming/quiescent division in massive galaxies. Luo et al. (2020) calculated a parabolic fit to mark the structural valley in the $\Sigma_1 - M_*$ plane, and $\Delta\Sigma_1$ is defined as the offset in $\log\Sigma_1$ from this line at fixed mass. With the mass trend removed, $\Delta\Sigma_1$ provides a more robust probe of the relationship between inner stellar mass surface density growth and global cold gas fraction.

When Σ_1 or $\Delta\Sigma_1$ is plotted against SFR, or alternatively against other parameters that trace SFR–such as

color, specific SFR (sSFR), or distance from the MS-a distinctive 'elbow' or 'L-shaped' pattern emerges in the distribution of galaxies in bins of M_* (Fang et al. 2013; Barro et al. 2017; Lee et al. 2018; Luo et al. 2020; Guo et al. 2021). It has been proposed that there is more than one possible track along which galaxies evolve as they transition from star-forming to quiescent. For example, in the plane of Σ_1 vs. sSFR, evolution may be characterized by either gas-rich or gas-poor quenching processes, which correspond to quenching at earlier and later times, respectively (Barro et al. 2013, 2017). For satellites, differences in evolution within this plane may involve quenching via bulge growth driven by central star formation, or through global mass-loss processes like tidal stripping (Woo et al. 2016). In any case, the consensus of the Σ_1 literature is that galaxies must build up their central bulge as a prerequisite for quenching.

The proposed mechanisms of massive galaxy quenching are too complex to discuss in depth here, and vary according to a variety of galaxy properties. Theoretical and simulation analyses contend that AGN feedback is a prominent – even necessary – mechanism for massive galaxy quenching (e.g. Croton et al. 2006; Dubois et al. 2013; Su et al. 2019; Piotrowska et al. 2021). Because of the close relationship between Σ_1 and the growth of the central black hole, we focus on the role of AGN feedback in gas removal and quenching and its connection to $\Delta\Sigma_1$.

It has been established that $f_{\rm H2}$ is tightly correlated with sSFR (Saintonge et al. 2017). In the plane of sSFR and $\Delta\Sigma_1$, galaxies follow a bimodal distribution which approximately separates star-forming from quiescent galaxies (Luo et al. 2020). These two relationships motivate us to investigate whether central bulge growth is also related to global cold gas content, particularly H_2 . Moreover, the scaling of cold gas content with Σ_1 has not been thoroughly explored in previous research. A few studies have analyzed the relationship between Σ_1 and cold gas content within the framework of cosmological simulations. Ma et al. (2022) and Khan et al. (2025) each concluded that Σ_1 is connected to a decline in cold gas in galaxy centers within the IllustrisTNG and NIHAO simulations, respectively, and offered AGN feedback as a plausible explanation. In this work, we will use observational data to compare the relationship between Σ_1 and global cold gas content to established gas scaling relations with M_* and μ_* . With the availability of molecular and atomic cold gas catalogs for representative samples, we are also positioned to explore the usefulness of Σ_1 and $\Delta\Sigma_1$ as indicators of galaxy quenching through an analysis of the cold gas reservoirs of galaxies with a range of $\Delta\Sigma_1$ values.

xGASS HI Sample

•	
Original xGASS Sample Size	1179
Cross-Matched with Σ_1 Catalog (Luo et al. 2020)	448
Emission-line fluxes with $S/N > 3$	370
Excluding code 3 or higher (i.e., confused) xGASS detections	341
Final Sample Size	341
Reliable Detections	213
Marginal Detections	19
Non-detections	109

Table 1. The original xGASS survey sample with detailed cuts made to the data set. The relative partitioning of our sample into reliable detections, marginal detections, and non-detections, or upper limits, is quantified.

In Section 2, we discuss our sample selection from archival data. Section 3 presents our analysis of the relationship between Σ_1 , AGN activity and gas content in our sample. In Section 4, we discuss our findings that Σ_1 is correlated with cold gas fraction above a certain threshold. We then connect the observed distribution of objects in the plane of $\Delta\Sigma_1$ vs. $f_{\rm H2}$ to existing observational and theoretical explanations for how galaxies evolve from star-forming to quiescent. Section 5 summarizes our results. Throughout this work, we assume a concordance $\Lambda{\rm CDM}$ cosmology: $H_0 = 70~{\rm km~s^{-1}~Mpc^{-1}}$, $\Omega_m = 0.3$, $\Omega_{\Lambda} = 0.7$.

2. SAMPLE SELECTION

The Extended GALEX Arecibo SDSS Survey (xGASS; Catinella et al. 2018) and Extended CO Legacy Database for GASS (xCOLDGASS; Saintonge et al. 2017) provide publicly available HI and H₂ catalogs for mass-selected samples of nearby galaxies. Spectral measurements were obtained from the MPA/JHU DR7 catalog¹ for the purposes of BPT classification (Brinchmann et al. 2004). The samples were then combined with Σ_1 data (Luo et al. 2020).

In Figure 1, we show the distribution of our HI and $\rm H_2$ samples in the SFR- M_* plane, compared to the SDSS DR7 Catalog (Abazajian et al. 2009). To identify galaxies as either star-forming or quiescent, we adopted the criterion set by Woo et al. (2015), who divided SDSS galaxies in the SFR- M_* plane according to the line $\rm log\,SFR=0.74\,log\,M_*-8.22$. Galaxies above this line are classified as star-forming, and those below it are considered quiescent. This line also fits our data well, even

xCOLDGASS H₂ Sample

Original xCOLDGASS Sample Size	532
Cross-Matched with Σ_1 Catalog (Luo et al. 2020)	226
Emission-line fluxes with $S/N > 3$	201
Final Sample Size	201
Detections	118
Non-detections	83

Table 2. The original xCOLDGASS survey sample with detailed cuts made to the data set. The distribution between detections and non-detections is quantified.

though the SFR values we use originate from a different source (the xGASS and xCOLDGASS catalogs).

2.1. Σ_1 Data

Luo et al. (2020) measured Σ_1 values for a volumeand mass-limited sample of > 40,000 SDSS galaxies. In particular, they focused on central galaxies with good viewing geometries, imposing the following restrictions: stellar mass $M_* > 10^{9.5} M_{\odot}$; axis ratio b/a > 0.5; Sérsic index 0.5 < n < 6; and redshift 0.02 < z < 0.07. See Luo et al. (2020) for details of their survey methods.

With the above restrictions, cross-matching our gas data with the Σ_1 data reduced our HI sample from the 1179 objects comprising the full xGASS catalog to 448, and reduced our H₂ sample from the original 532 objects of the xCOLDGASS sample to 226.

Since we are using the Σ_1 values calculated by Luo et al. (2020), we use the same stellar mass data for consistency, which are obtained from the MPA/JHU DR7 value-added catalog. We also adopt their computed $\Delta\Sigma_1$ values in our analysis.

2.2. HI sample

xGASS is a targeted survey of galaxies with $10^9 M_{\odot}$ < $M_* < 10^{11.5} M_{\odot}$ and redshifts 0.01 < z < 0.05. Integration times were set by the requirement that certain upper limits be reached unless a measurement could be obtained with a sufficient S/N ratio, allowing for greater sensitivity in the low $f_{\rm HI}$ regime. The distribution of galaxies is approximately uniform in stellar mass bins between $\log M_*/M_{\odot} = 10 - 11$, and decreases steadily for $\log M_*/M_{\odot} > 11$. The representative sample contains 1179 galaxies, a fraction of which are galaxies with archival HI data obtained from ALFALFA or the Cornell HI Archive, which were not remeasured for survey efficiency. For further information on how HI data were collected and chosen for the xGASS sample, see Catinella et al. (2018), and for general GASS survey methods, see Catinella et al. (2010) and Catinella et al. (2013).

¹ https://wwwmpa.mpa-garching.mpg.de/SDSS/DR7/

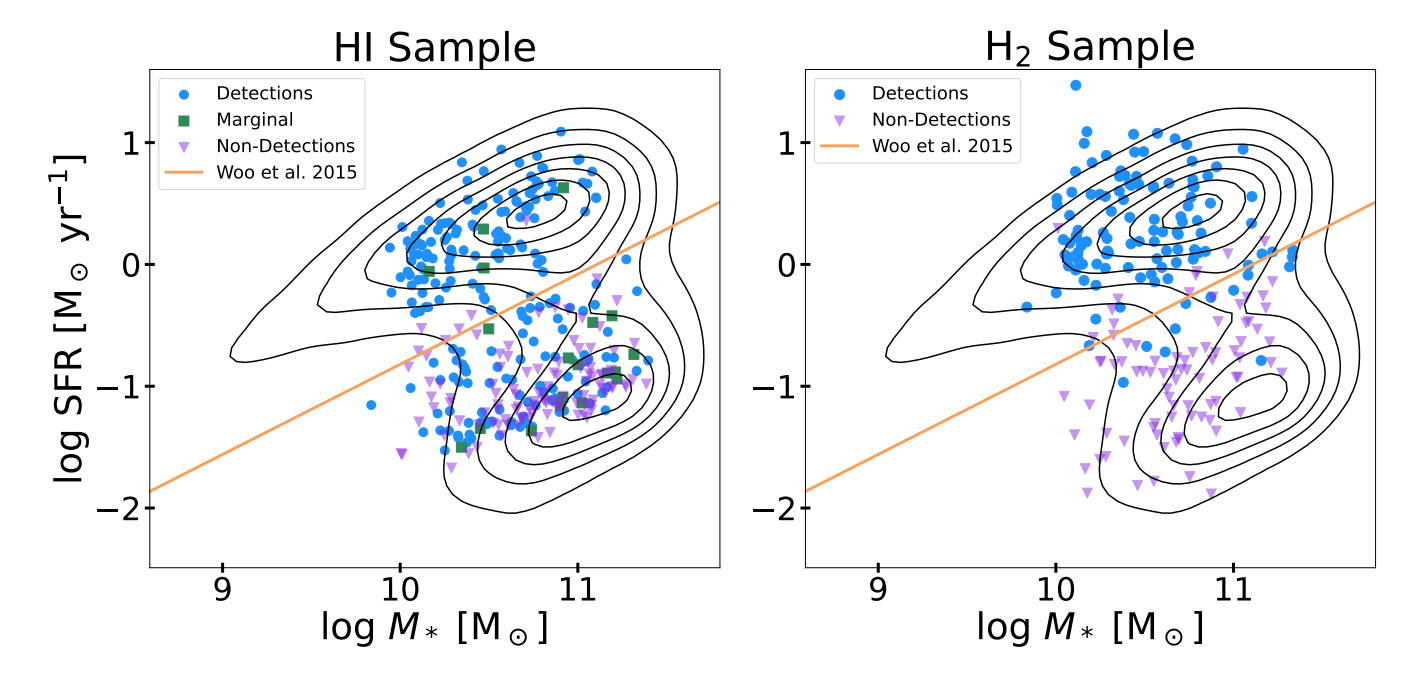


Figure 1. (Left) The contours represent the SDSS main sample on the SFR- M_* plane, and we include the line from Woo et al. 2015 to indicate objects that are either star-forming (above the line) or non-star-forming (below the line). The points comprise our final HI sample from the original xGASS sample. Code 2 xGASS detections are square markers to distinguish them as "less reliable" or "marginal" detections. (Right) The contours of the full SDSS sample are now overlaid with the points comprising our H_2 sample, which was derived from the full xCOLDGASS sample. In both plots, non-detections are indicated by triangle markers. For further explanation, see Sections 2.2 and 2.3.

For the purposes of this work, we consider both HI detections and non-detections. Non-detections are listed with 5σ upper limits in the xGASS tables. If measured by GASS, the highest quality, or "code 1" detections, were detected with S/N $\gtrsim 6.5$ and are considered reliable (Catinella et al. 2018). Code 3 or higher HI detections are flagged by Catinella et al. (2018) as being "marginal and confused" or simply "confused". For these targets, HI emission is believed to originate from a different source within the beam. There are a total of 74 such measurements in the full xGASS sample.

Code 2 detections are marginal in that they have lower S/N (between 5 and 6.5) compared to code 1 detections. They are *not* confused, and as such they can be considered secure detections, albeit with more uncertain HI masses. In our figures, code 2 detections are labeled separately from the sample of code 1 xGASS detections and high-confidence archival measurements. There are 19 objects in our sample that fall into this category. The motivation to include these points graphically is to provide more coverage of the parameter space. However, in calculating sample statistics such as averages, these points are excluded.

Table 1 offers an analysis of all cuts made to the original HI xGASS sample, for a final sample size of 341. We compare the distributions of M_* , μ_* and SFR within our

sample to the xGASS sample in Figure 2. Figure 1 shows the distribution of these objects in the SFR- M_* plane. As expected, galaxies along the MS are largely detected in HI, while galaxies lacking HI detections cluster in the passive sequence.

2.3. H_2 sample

We extract our $\rm H_2$ data from the xCOLDGASS sample, which spans a mass of $10^9 < M_*/M_\odot < 10^{11.5}$ and redshift range of 0.01 < z < 0.05 (Saintonge et al. 2017). The methods of xCOLDGASS are complementary to those of xGASS, and there are 477 galaxies common to both samples.

In xCOLDGASS, $\rm H_2$ masses are extrapolated from CO(1-0) emission line flux measurements, which serve as a tracer for molecular gas. For details about the sampling and detection methods of xCOLDGASS, see Saintonge et al. (2017). Non-detections are reported with 3σ upper limits in the xCOLDGASS tables, and all detections have S/N > 5 by survey design. Within our sample, there are 118 detections and 83 non-detections.

Table 2 offers an analysis of the cuts we made to our sample, for a final sample size of 201. We compare the distributions of M_* , μ_* and SFR within our H_2 sample to the xCOLDGASS sample in Figure 2. The distribution of these objects in the SFR- M_* plane is shown on the right in Figure 1. As with our HI sample, passive

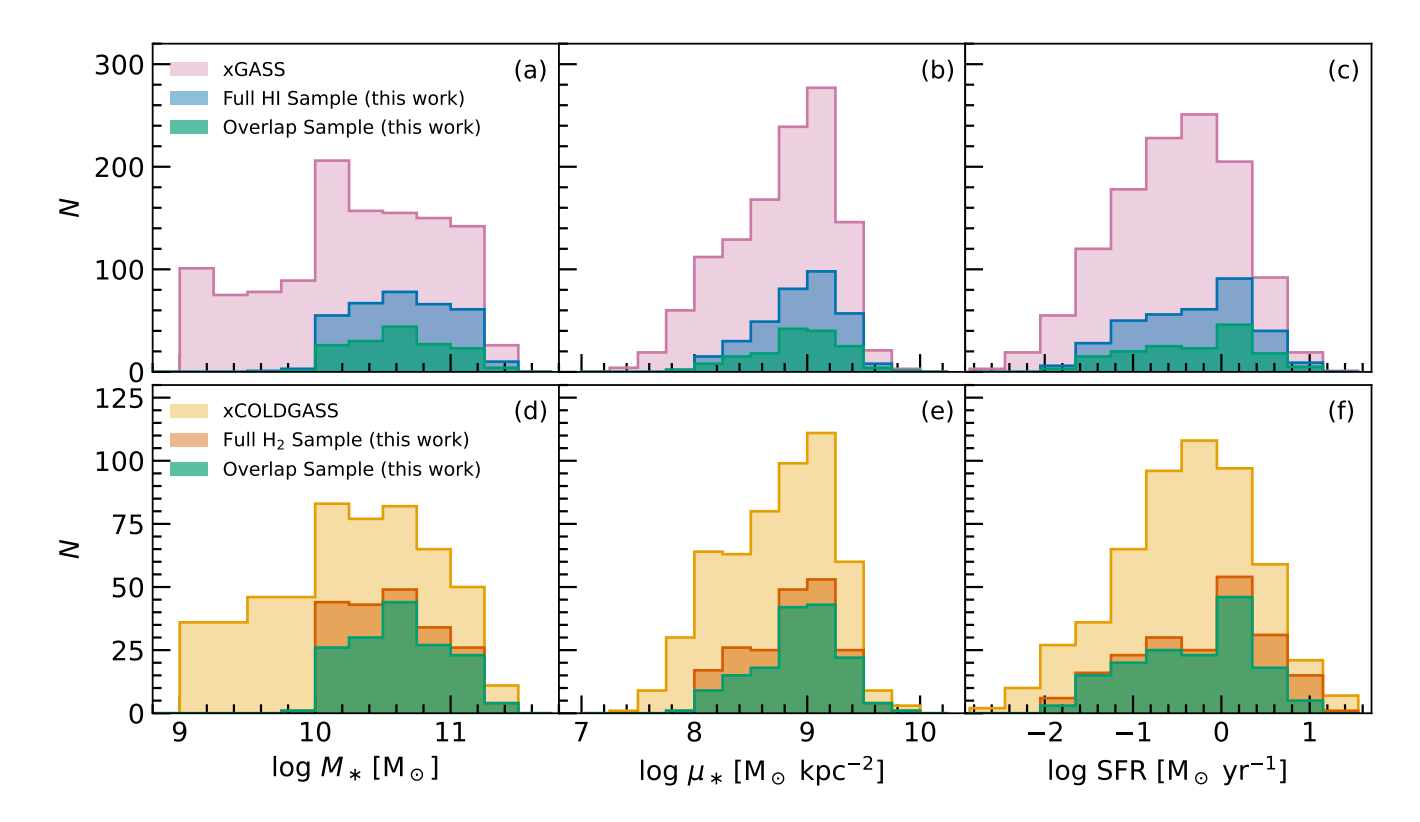


Figure 2. The distributions of (a) M_* , (b) μ_* and (c) SFR are compared between the xGASS sample, our HI sample, and the overlap sample, which consists of the 155 galaxies common to our HI and H₂ samples. (d-f) The distributions of these three key properties are compared between the xCOLDGASS sample, our H₂ sample, and the overlap sample.

galaxies predominantly lack detections, while nearly all star-forming galaxies are detected in H₂.

2.4. Our Samples in the BPT Diagram

A central focus of this paper is on quantifying the relationship between AGN activity, $\Delta\Sigma_1$ and cold gas fractions. Emission-line fluxes and their errors for [OIII], [NII], $H\alpha$ and $H\beta$ were extracted from the MPA/JHU DR7 catalog of spectral measurements for the purposes of BPT classification (Baldwin et al. 1981). We impose the condition that S/N > 3 for each line. Upon enforcing this restriction, our samples were reduced to 370 objects with HI data and 201 objects with H₂ data.

Figure 3 shows the distribution of our sample in the BPT diagram. There are fewer star-forming galaxies, demarcated by their location below the Kauffmann et al. (2003) line, than typically observed for larger, more representative samples. There is a documented mass trend within the BPT diagram whereby the star-forming branch is dominated by lower-mass galaxies (e.g. Kumari et al. 2021); since our sample is limited to higher-mass objects (log $M_*/M_{\odot} \gtrsim 10$), the distribution of star-forming galaxies is lacking, particularly for log([NII]/H α) < -0.6.

Galaxies located above the Kewley et al. (2001) line are classified as AGN candidates. Our HI sample contains 163 such candidates (48% of the sample) and our H₂ sample contains 85 (42%). We note that AGN are somewhat overrepresented in our sample compared to the Luo et al. (2020) sample, in which $\sim 35\%$ of galaxies meeting their selection criteria are AGN for $M_* > 10^{10} M_{\odot}$ and $0.02 \le z \le 0.05$. This is discussed further in Section 3.4.

2.5. Overlap Sample

Because our HI and $\rm H_2$ samples are drawn from two surveys with different selection criteria, it is important to determine the extent to which our two samples exhibit similar distributions in key parameters. This is done to assess the robustness of our main results against potential sample biases. There are 155 galaxies that are common to both samples (the "overlap sample"). Of these, 103 have HI detections and 86 have $\rm H_2$ detections.

Figure 2 presents the distributions in M_* , μ_* , and SFR for our HI and H₂ samples and compares them with the distributions of the parent xGASS and xCOLDGASS samples. Our samples are consistent with the underlying xGASS and xCOLDGASS samples, indicating that our

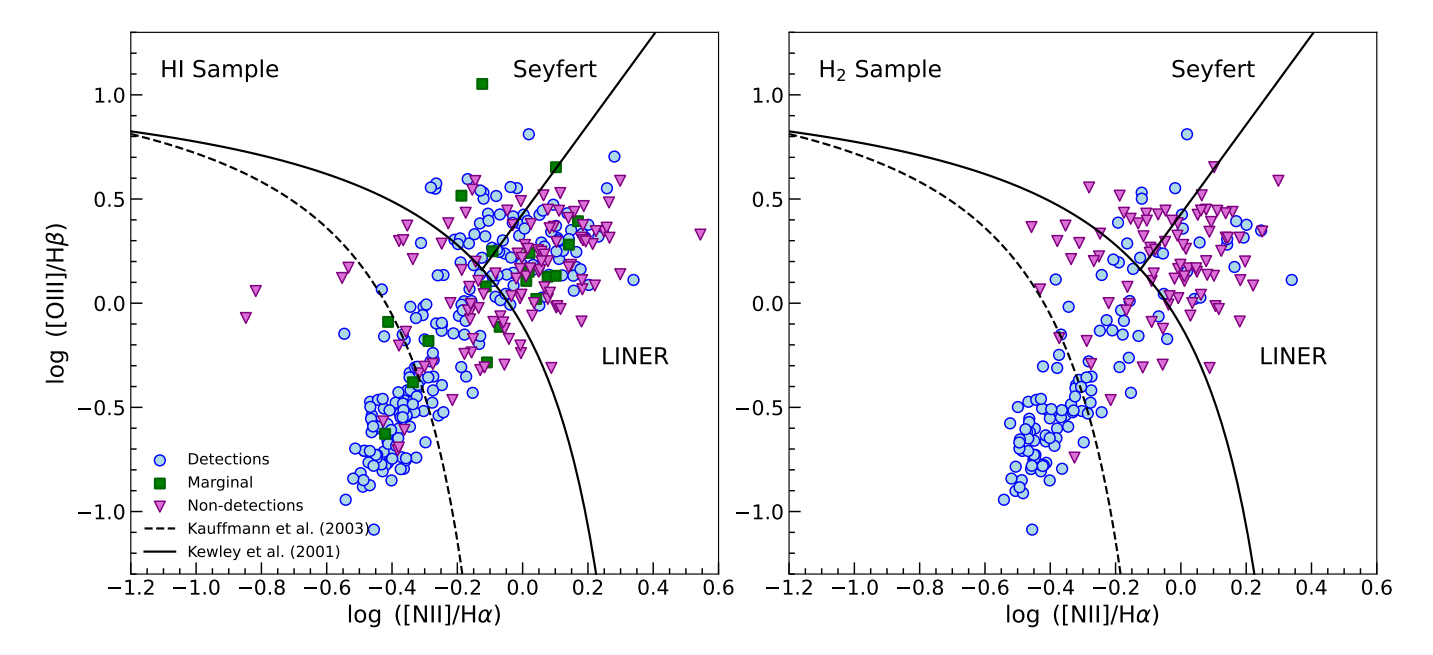


Figure 3. (*Left*) The BPT diagram for our HI sample, and (*right*) for our H₂ sample. We show the theoretical relation of Kewley et al. (2001) and empirical relation of Kauffmann et al. (2003), which separate galaxies based on their dominant source of gas ionization.

selection criteria have not introduced any biases in these parameters.

Also shown in Figure 2 are the distributions for the overlap sample. In general, the overlap sample has similar distributions to our HI and H₂ samples. One notable discrepancy is in stellar mass. This is made clearer in Figure 4, which compares the distributions for the HI, H_2 , and overlap samples directly. More than 75% of galaxies in our full H₂ sample are also in the HI sample, but we find that our full H₂ sample is slightly biased toward lower masses compared to both the HI and overlap samples. This can be attributed to the differing distributions in M_* between the xGASS and xCOLDGASS samples (Figure 2). We also note that galaxies with masses between $10 < \log(M_*/M_{\odot}) < 10.25$ appear to be underrepresented in our HI sample compared to the xGASS sample (Figure 2). These discrepancies notwithstanding, we show below that they do not affect our results.

3. RESULTS

3.1. Statistical Methods

Since our samples include objects with low SFR (and presumably low gas content), it is important that we properly treat objects in our samples that have non-detections in HI and/or $\rm H_2$. It is common to use statistical methods such as survival analysis or spectral stacking to robustly treat upper limits for the purposes of including them in data analysis. For a recent overview of such methods in astronomy, see Saintonge & Catinella (2022).

Within bins of Σ_1 or $\Delta\Sigma_1$, the detection rate was as low as 20%. The median of the distribution is not meaningful in such cases. The Kaplan-Meier (KM) estimator, a non-parametric statistic used in survival analysis, can provide feasible sample statistics down to a detection rate of approximately 20%, albeit with greater uncertainty. In order to include upper limits in our analysis, we elect to use the KM estimator to compute means in the gas fraction within bins of the independent variable in our analyses, adhering to the methods of Feigelson & Nelson (1985). We simulated uncertainty in the gas fraction by bootstrapping; the data was resampled 1000 times with replacement, and the survival function and resulting binned average gas fractions were recomputed for each trial. We use the 5th and 95th percentiles in the distribution of gas fraction means for the 1000 trials to assign a measure of confidence to the "true" gas fraction means estimated via the KM estimator.

Quantifying the slope or scatter of a linear trend is also challenging in the presence of upper limits, when traditional methods are no longer valid. Consequently, we apply the Bayesian hierarchical model for linear regression implemented in the IDL procedure LINMIX_ERR (Kelly 2007). This method is capable of fitting a straight line to data which includes non-detections in the y variable, making it a suitable choice for our study. In addition to linear regression parameters, LINMIX_ERR returns the Gaussian intrinsic scatter of the dependent variable about the regression line. This method has been used widely in astronomy (e.g. Bentz et al. 2013; Mc-

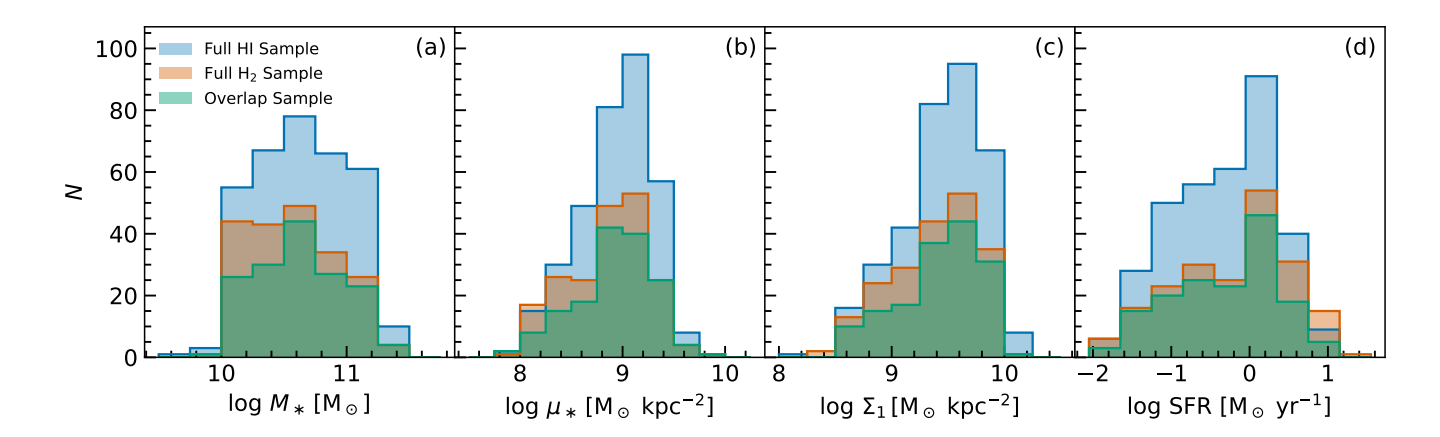


Figure 4. We show the distributions of (a) M_* , (b) μ_* , (c) Σ_1 , and (d) SFR for our HI and H₂ samples. The distributions are not identical for these four parameters, so we utilize the overlap sample consisting of the galaxies common to both of our samples to examine the robustness of our results. This is particularly relevant for our investigations of Σ_1 and $\Delta\Sigma_1$ vs. cold gas fraction.

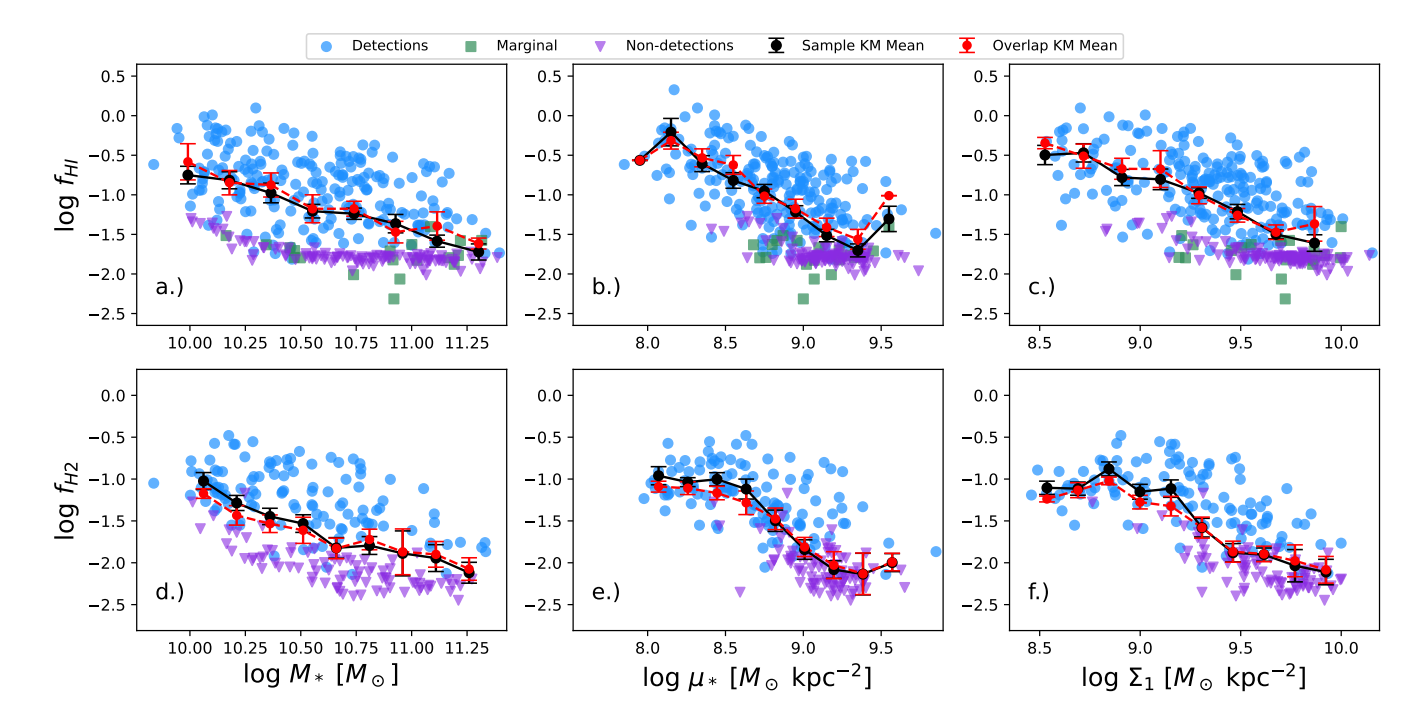


Figure 5. Gas fractions $f_{\rm HI}$ and $f_{\rm H2}$ plotted against Σ_1 , M_* , and μ_* . (Top Row) xGASS HI detections are blue circular markers, marginal detections are green square markers, and non-detections, or upper limits, are purple triangular markers. (Bottom Row) Blue circular points represent xCOLDGASS H₂ detections and purple triangular markers indicate upper limits. Black markers indicate the Kaplan-Meier means of the individual samples (non-detections and detections, excluding marginal ones), while the red markers indicate the Kaplan-Meier means of the overlap sample.

Connell & Ma 2013), and it has recently been applied to xCOLDGASS data (Hagedorn et al. 2024). For details about the method itself, see Kelly (2007).

In the remainder of this section, the dependence of cold gas content on Σ_1 is compared with the dependencies on μ_* and M_* , as these parameters have well-established relationships with cold gas content. We then examine the connection between $\Delta\Sigma_1$, gas fraction, and BPT classification. In all plots, a minimum of 10 points is required in each bin.

3.2. Σ_1 and Cold Gas Fraction

In the top row of Figure 5, we plot $f_{\rm HI}$ vs. stellar mass and structural parameters μ_* and Σ_1 . We confirm previously established findings that $f_{\rm HI}$ is negatively correlated with M_* and μ_* for nearby galaxies (e.g. Catinella et al. 2010; Huang et al. 2012; Kauffmann et al. 2012; Brown et al. 2015; Catinella et al. 2018; Hunt et al. 2020). We find that there is a similarly strong dependence of $f_{\rm HI}$ on Σ_1 .

In agreement with Saintonge et al. (2017), we observe negative correlations between $f_{\rm H2}$ and both M_* and μ_* in the bottom row of Figure 5. We similarly note considerable scatter in the dependence of $f_{\rm H2}$ on M_* , with an intrinsic scatter of approximately 0.43 dex.

The trend between Σ_1 and $f_{\rm H2}$ is similar to the observed trend between μ_* and $f_{\rm H2}$, which intuitively makes sense because of the close relation between these measurements. A mild 'elbow' shape emerges in both planes, suggesting nonlinear behavior. The H₂ fraction, as measured by the KM means, exhibits little dependence on Σ_1 when $\Sigma_1 < 10^9 M_{\odot} \text{ kpc}^{-2}$, but for $\Sigma_1 > 10^9 \ M_{\odot} \ \mathrm{kpc}^{-2}$, $\log f_{\mathrm{H2}}$ decreases almost linearly with $\log \Sigma_1$. In this regime, we find that the relationship between $\log f_{\rm H2}$ vs. $\log \Sigma_1$ can be described by a line with a slope of -1.32 ± 0.08 and an intrinsic scatter of 0.38 ± 0.01 dex. Similarly, the mean value of $\log f_{\rm H2}$ decreases by about 1 dex in the range of $\mu_* \sim 10^{8.5} - 10^{9.5} M_* \text{ kpc}^{-2}$. This is consistent with the expected decline in molecular gas in bulge-dominated galaxies.

We find that $\log f_{\rm HI}$ also decreases linearly with $\log \Sigma_1$ for $\Sigma_1 > 10^9~M_{\odot}~{\rm kpc}^{-2}$, with a slope of -1.11 ± 0.07 and an intrinsic scatter of 0.42 ± 0.01 dex. Interestingly, $\log f_{\rm HI}$ vs. $\log \Sigma_1$ does not exhibit nonlinear behavior to the extent we observe for $\log f_{\rm H2}$ vs. $\log \Sigma_1$. We elaborate on this observation in Section 4.1.

3.3. $\Delta\Sigma_1$ and Cold Gas Fraction

In Figure 6, we show the distribution of our samples in the plane of gas fraction vs. $\Delta\Sigma_1$ color-coded by sSFR. The parameter $\Delta\Sigma_1$ is defined as the offset in $\log\Sigma_1$

relative to the "structural valley", a feature in the plot of $\log \Sigma_1$ vs. $\log M_*$ which generally separates bulge-dominated from disk-dominated galaxies at fixed mass (Luo et al. 2020). The bin widths are approximately 0.12 dex in $\Delta \Sigma_1$ in both samples.

We observe an 'elbow' pattern in the plane of $f_{\rm H2}$ vs. $\Delta\Sigma_1$, a shape that often emerges in the planes of star formation or color vs. Σ_1 or $\Delta\Sigma_1$ (Fang et al. 2013; Barro et al. 2017; Lee et al. 2018; Luo et al. 2020; Guo et al. 2021). Following the trend in KM means, the H_2 fraction exhibits minor variation until just before $\Delta\Sigma_1=0$, at which point the mean fraction decreases by an order of magnitude over an interval of $\Delta\Sigma_1\approx 0.4$ dex. This trend is also seen in the overlap sample (Figure 6).

We observe that the trend between $\Delta\Sigma_1$ and $f_{\rm H2}$ is steeper than the relationship between $\Delta\Sigma_1$ and $f_{\rm HI}$ in the vicinity of the $\Delta\Sigma_1 = 0$ point. To quantify this, we apply the LINMIX_ERR method to fit a line to the data in the regime of $-0.2 < \log \Delta \Sigma_1 < 0.2$, where it is still possible to fit a line, within error, to the KM means. We find that the slope between $\log f_{\rm H2}$ and $\log \Delta \Sigma_1$ is -2.57 ± 0.29 , compared to a slope of -2.16 ± 0.21 between $\log f_{\rm HI}$ and $\log \Delta \Sigma_1$. For the overlap sample, we obtain results consistent with these values, so our finding that the slope observed for $\log f_{\rm H2}$ vs. $\log \Delta \Sigma_1$ is steeper than the log $f_{\rm HI}$ vs. log $\Delta\Sigma_1$ slope is robust against possible sampling bias due to the different samples. Our observation that the $\Delta\Sigma_1 - f_{\rm H2}$ trend is steeper than its $f_{\rm HI}$ counterpart around the $\Delta\Sigma_1 = 0$ point suggests that the molecular gas fraction may be more sensitive to changes in Σ_1 at fixed mass, particularly where galaxies cross the $\Sigma_1 - M_*$ structural valley.

In agreement with Luo et al. (2020), we find that there is a critical point marked by $\Delta\Sigma_1 = 0$ after which point star formation is generally suppressed. This is illustrated in Figure 6, where the shading of points indicates that sSFR declines with increasing $\Delta\Sigma_1$ and with decreasing $f_{\rm HI}$ and $f_{\rm H2}$. Galaxies with lower sSFR are found preferentially where $\Delta\Sigma_1 > 0$.

To quantify this, we employ the star-forming criterion of Woo et al. (2015) to define the fraction of quenched objects as a function of $\Delta\Sigma_1$ (Figure 6). Among galaxies with $\Delta\Sigma_1 > 0$, we find that 65.6% of our HI sample and 62.3% of our H₂ sample are quiescent. In contrast, only 7.2% and 5.6% of galaxies with $\Delta\Sigma_1 < 0$ are quiescent in our HI and H₂ samples, respectively. Consequently, we contend that $\Delta\Sigma_1 = 0$ approximately marks a transition from star-forming to quiescent galaxies.

3.4. AGN Activity

In Figure 7, we show the distribution of Seyfert and LINER host candidates in the plane of cold gas fraction

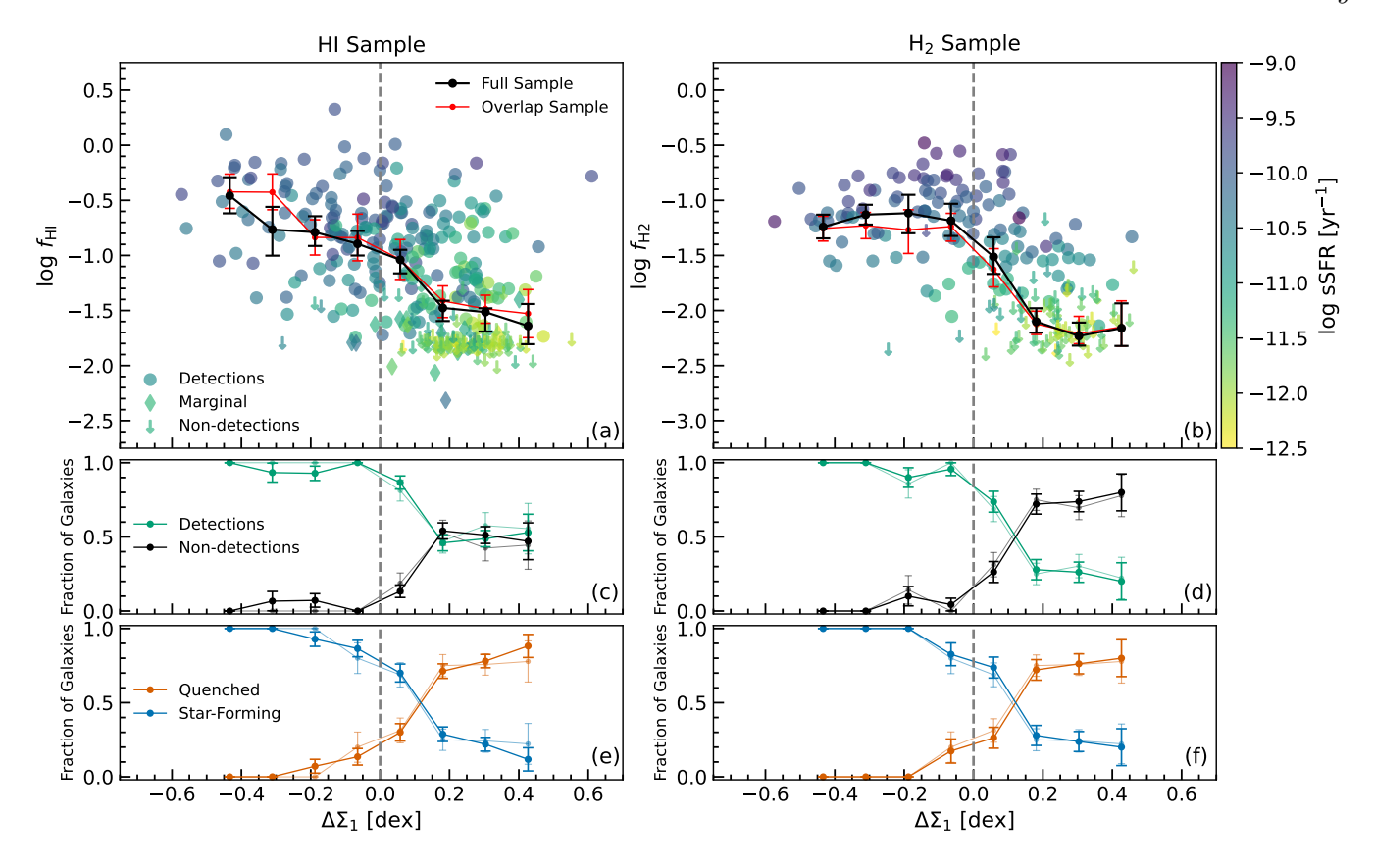


Figure 6. The dependence of (a) $f_{\rm HI}$ and (b) $f_{\rm H2}$ on the relative parameter $\Delta\Sigma_1$, coded by specific SFR. The black points represent the mean $f_{\rm HI}$ and $f_{\rm H2}$ values computed using survival analysis techniques within bins of $\Delta\Sigma_1\approx 0.12$ dex. The red points represent the mean values within the overlap sample. Error bars are the 5th and 95th percentiles in the bootstrap distribution as described at the beginning of Section 3. (c-d) For both samples, we plot the fraction of galaxies with gas detections and the fraction without as a function of $\Delta\Sigma_1$, relative to the total number of galaxies within a given bin of $\Delta\Sigma_1$. For (c) the HI sample, we count marginal detections as detected. (e-f) The fraction of quenched and star-forming galaxies as a function of $\Delta\Sigma_1$. Galaxies are defined as star-forming or quenched according to the SFR- M_* line defined by Woo et al. 2015. In plots (c-f), error estimates are obtained via bootstrapping. The thinner, transparent lines indicate the relevant fractions in the overlap sample. The trends shown in (c-f) for the full samples are identical (within the uncertainties) to those found using the overlap sample.

vs. $\Delta\Sigma_1$. For galaxies that have $\Delta\Sigma_1 > 0$, we find that 60.2% of the HI sample and 58.5% in the H₂ sample are classified as AGN host candidates (either Seyfert or LINER), while just16.5% and 12.7% of all galaxies with $\Delta\Sigma_1 < 0$ are AGN candidates in our HI and H₂ samples, respectively.

While AGN are overrepresented in our sample compared to the Luo et al. (2020) sample (Section 2.4), the general trend is the same between their sample and ours; there is an increase in AGN activity for $\Delta\Sigma_1 > 0$, and little AGN activity for $\Delta\Sigma_1 < 0$. Within the Luo et al. (2020) sample of galaxies – after we impose the constraints that $M_* > 10^{10} M_{\odot}$ and $0.02 \le z \le 0.05$ to be consistent with our samples – approximately 50% of the galaxies located above the $\Sigma_1 - M_*$ structural valley ($\Delta\Sigma_1 > 0$) are AGN candidates, compared to $\approx 12\%$ of galaxies below. This suggests that AGN candidates are

possibly overrepresented in our samples for $\Delta\Sigma_1 > 0$. Regardless, in both our sample and the parent sample, we can conclude that the threshold $\Delta\Sigma_1 > 0$ is associated with a greater incidence of AGN candidates relative to the region $\Delta\Sigma_1 < 0$.

To further visualize the connection between AGN activity, inner stellar surface mass density and gas depletion, we separately track the relative proportion of Seyfert/LINER candidates in bins of $\Delta\Sigma_1$ in panels (e) and (f) of Figure 7. Uncertainties in the binned fractions are obtained via bootstrapping.

We investigate Seyfert and LINER trends separately due to the fact that many LINERs may be produced by ionization due to post-AGB stars rather than AGN (e.g. Singh et al. 2013). To supplement the BPT diagram, previous works have imposed the additional constraint that galaxies have an H α equivalent width EW_{H α} >

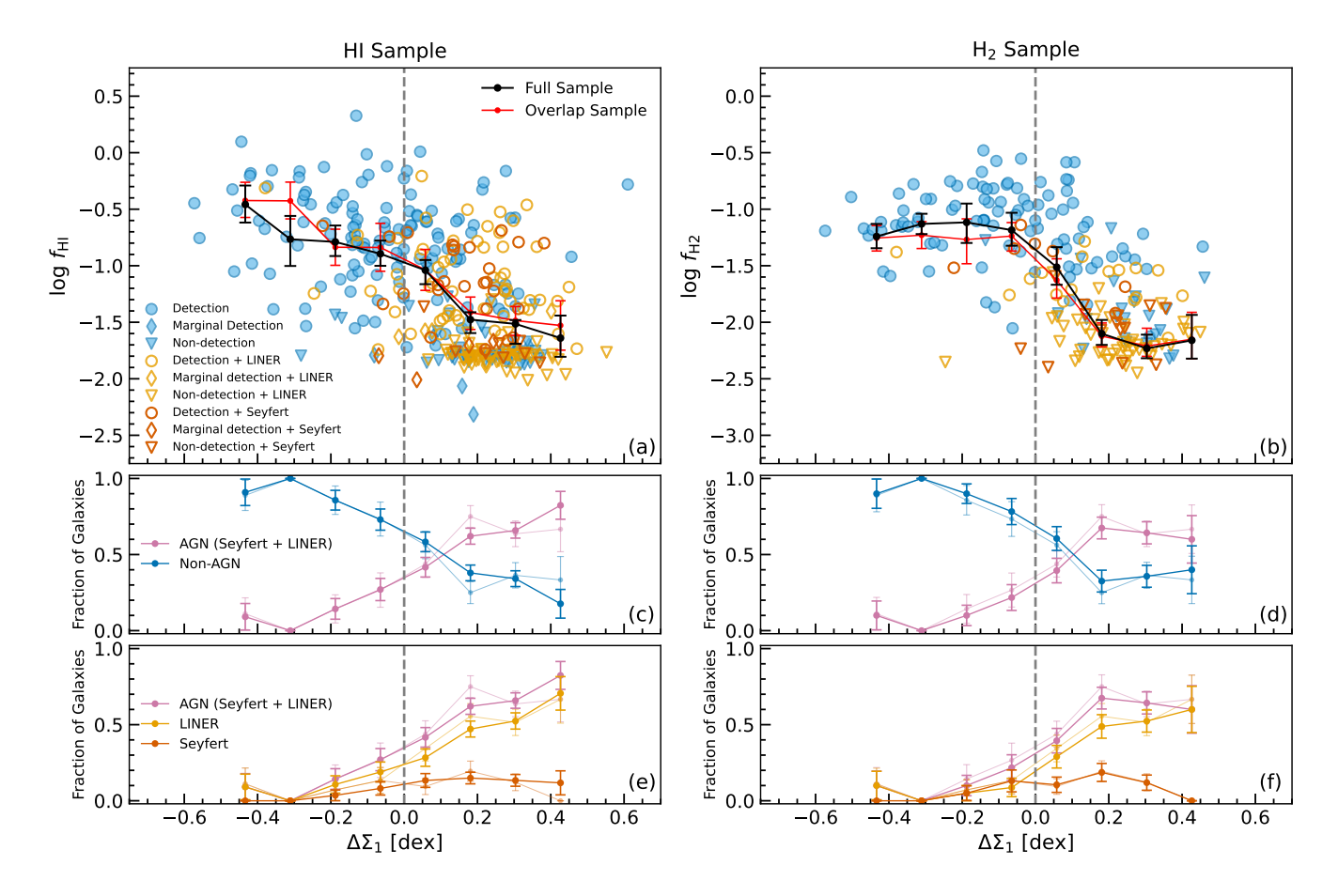


Figure 7. The dependence of (a) $f_{\rm HI}$ and (b) $f_{\rm H2}$ on the relative parameter $\Delta\Sigma_1$, coded by Seyfert or LINER classification. The black points represent the mean $f_{\rm HI}$ and $f_{\rm H2}$ values computed using survival analysis techniques. Open red markers are Seyfert candidates and open orange markers are LINER candidates selected based on their position in the BPT diagram. Blue points represent those galaxies not classified as AGN. (c-d) The fraction of galaxies within bins of $\log \Delta\Sigma_1$ that are classified as AGN candidates and the fraction of galaxies that are not are plotted for our (c) HI sample and our (d) H₂ sample. (e-f) The fraction of galaxies that are classified as Seyfert or LINER as a function of $\Delta\Sigma_1$. For reference, the total AGN fraction per bin is also shown. Error estimates in (c-f) are obtained via bootstrapping. The thinner, transparent lines in (c-f) indicate the relevant fractions in the overlap sample. The trends shown for the full samples are identical (within the uncertainties) to those found using the overlap sample.

3 Å to be considered genuine AGN (Fernandes et al. 2010; Cid Fernandes et al. 2011). We compute $EW_{H\alpha}$ values for the LINERs in our HI and H_2 samples from the MPA/JHU DR7 catalog. We find that only $\sim 10\%$ and $\sim 8\%$ of the LINERs have $EW_{H\alpha} > 3$ Å in our HI and H_2 samples, respectively. For this reason, we caution the reader against interpreting our LINER sample as genuine AGN, but rather as weak AGN candidates or retired galaxies.

We find that Seyfert activity peaks at $\Delta\Sigma_1 \approx 0.2$ dex, and the abundance of LINER hosts increases greatly between $\Delta\Sigma_1 \approx 0$ and 0.2 dex (Figure 7). Overall, > 60% of galaxies that have $\Delta\Sigma_1 > 0.2$ dex are AGN candidates, which indicates that elevated central surface mass density at fixed mass is associated with a higher likelihood of AGN activity.

4. DISCUSSION

4.1. The Relationship between Σ_1 and Cold Gas

Our findings suggest that Σ_1 is anti-correlated with both $f_{\rm HI}$ and $f_{\rm H2}$ for $\Sigma_1 > 10^9~M_{\odot}~{\rm kpc}^{-2}$. However, the trends between the mean atomic and molecular gas fractions and Σ_1 , shown by the red points in panels (c) and (f) of Figure 5, are notably different, mirroring the relationship between gas fraction and μ_* . For $\Sigma_1 < 10^9~M_{\odot}~{\rm kpc}^{-2}$, the trend between $f_{\rm H2}$ and Σ_1 is flat, but there is a quantifiable decline of approximately 1 dex in $f_{\rm H2}$ for $10^9 < \Sigma_1/(M_{\odot}~{\rm kpc}^{-2}) < 10^{10}$. The relationship between $f_{\rm HI}$ and Σ_1 does not appear to adhere to an 'elbow' shape which would suggest nonlinear behavior. Although the correlation is weak for $\Sigma_1 < 10^9~M_{\odot}~{\rm kpc}^{-2}$, the mean atomic gas fraction gen-

erally follows a decreasing trend across the full range of Σ_1 , which is not the case for $f_{\rm H2}$. Because $f_{\rm H2}$ appears to change only at a particular threshold in Σ_1 , we postulate that the molecular gas fraction may be more directly affected by the growth of the central bulge than the atomic gas fraction.

As the detected sample consists predominantly of main-sequence galaxies, this observation could be explained by appealing to the typical galactic distribution of cold gas in massive disk galaxies. HI is accreted into the outskirts of galaxies via gas infall from the intergalactic medium or cosmic filaments, after which point it can replenish the inner parts of the galaxy and fuel star formation via conversion into the molecular phase (see e.g. Sancisi et al. (2008) for a review of cold gas accretion). As a result, the centers of nearby spiral galaxies are dominated by H₂ gas, while the outskirts are dominated by HI gas (Young & Scoville 1991; Bigiel et al. 2008; Leroy et al. 2008). Since Σ_1 probes the central regions of galaxies, we expect $f_{\rm H2}$ to exhibit greater sensitivity to Σ_1 than $f_{\rm HI}$. This is further supported by the more direct connection between $\Delta\Sigma_1$ and $f_{\rm H2}$ compared to $f_{\rm HI}$, which is discussed in depth in the next subsection. However, it should be noted that the mild 'elbow' shape observed in the plane of $f_{\rm H2}$ vs. Σ_1 could be a byproduct of the tighter correlation between $f_{\rm H2}$ and SFR, and of the nonlinear behavior which has been reported between Σ_1 and sSFR (e.g. Barro et al. 2013).

4.2. $\Delta\Sigma_1$ as an Indictor of Evolution Towards Quenching

Previous literature has proposed that galaxies evolve towards higher Σ_1 and that galaxies quench at some mass-dependent threshold (Fang et al. 2013; van Dokkum et al. 2015; Barro et al. 2017). Luo et al. (2020) contended that $\Delta\Sigma_1 = 0$ is the demarcation between pseudo-bulges, which lie to the left of $\Delta\Sigma_1 = 0$, and classical bulges, which lie to the right. They observed a "bimodality" in the distribution of $\Delta\Sigma_1$ vs. global sSFR, whereby galaxies to the left of $\Delta\Sigma_1 = 0$ have systematically greater values of sSFR, while galaxies to the right have lower values, but with some range in sSFR. Luo et al. (2020) raised the possibility that some galaxies evolve from pseudo- to classical-type bulges, or from low to high $\Delta\Sigma_1$, and as such they offered an explanation for the greater range of sSFR values to the right of $\Delta\Sigma_1 = 0$ as the result of differences in structure and stellar populations during evolution towards quenching.

We observe a decrease in both $f_{\rm H2}$ and $f_{\rm HI}$ across $\Delta\Sigma_1=0$, and a corresponding decrease in sSFR (Figure 6). While $f_{\rm HI}$ exhibits an approximately linear decline with $\Delta\Sigma_1$, $f_{\rm H2}$ decreases nonlinearly with $\Delta\Sigma_1$, partic-

ularly across the $\Delta\Sigma_1$ zero point as discussed in Section 3.3. This makes sense in light of the fact that the central gas reservoir is dominated by molecular gas, as discussed in Section 4.1. Additionally, there is evidence to suggest that H_2 content is more tightly correlated with galaxy quiescence than HI. Zhang et al. (2019) observed evidence for significant HI gas reservoirs in nearby, massive quiescent galaxies which were classified as centrals with disk morphology. A significant proportion of their sample had HI detections but were generally depleted in H_2 gas.

In accordance with Luo et al. (2020), we find that $\Delta\Sigma_1$, like Σ_1 , is indicative of quenching, and furthermore, that $\Delta\Sigma_1$ may be indicative of evolution towards quenching. It is tempting to consider that the mean trend of $\Delta\Sigma_1$ vs. $f_{\rm H2}$ in Figures 6 and 7 constitutes an evolutionary track; in the remainder of this subsection, we show that this is plausible.

We observe that sSFR systematically decreases with $f_{\rm H2}$ and $\Delta\Sigma_1$, and that where the mean trend line crosses the $\Delta\Sigma_1=0$ point in Figure 6, sSFR $\sim 10^{-11} {\rm yr}^{-1}$. The delineation between star-forming and quiescent galaxies as shown in Figure 1 corresponds to sSFR $\sim 10^{-11} {\rm yr}^{-1}$; hence, $\Delta\Sigma_1=0$ also approximately marks the quenching point along the mean trend line.

Fang et al. (2013) contend that the key evolutionary driver of quenching for massive, central galaxies in the local Universe is the build-up of central mass surface density at roughly fixed global stellar mass. An evolutionary track within the plane of $\Delta\Sigma_1$ vs. $f_{\rm H2}$ must therefore generally occur in the direction of increasing $\Delta\Sigma_1$, at least before the quenching point. While there are processes which can reduce Σ_1 , the effects are generally minor and occur after quenching (van Dokkum et al. 2015; Barro et al. 2017). Together with the fact that sSFR should decline as galaxies quench, then galaxies on this evolutionary track must also be declining in sSFR. The mean trend of Figure 6 fulfills these criteria. Within this interpretation, then on average, H₂ gas is depleted more quickly at fixed mass than HI gas within the vicinity of the quenching point, $-0.2 \, \mathrm{dex} \lesssim \log \Delta \Sigma_1 \lesssim 0.2 \, \mathrm{dex}$. This implies that molecular gas is depleted faster than atomic gas as galaxies evolve towards quenching, as marked by central bulge growth. Popping et al. 2015 shows that molecular gas evolves much more rapidly than atomic gas over cosmic time, with $f_{\rm H2}$ declining strongly while HI remains nearly constant at fixed stellar mass. In our nearbygalaxy sample, we find the same trend in the rate of change: $f_{\rm H2}$ drops steeply across the $\Delta\Sigma_1 = 0$ transition, whereas $f_{\rm HI}$ decreases more gradually.

We caution against interpreting the mean trend as a single evolutionary track; it is possible that there are multiple evolutionary tracks within the $f_{\rm H2}-\Delta\Sigma_1$ plane, a point which we refer to in the next subsection. Additionally, there may be exceptions to our assumptions of galaxies building up their central bulges at fixed mass. Deviations from the fixed-mass, bulge-growth picture could be an additional source of scatter in our data.

Ma et al. (2022) employed cosmological simulations to examine how $\Delta\Sigma_1$ correlates with offsets in cold gas massspecifically, $\Delta \log M_{\rm HIMS}$ and $\Delta \log M_{\rm H_2MS}$ where each is defined as the deviation in either $M_{\rm HI}$ or $M_{\rm H_2}$ from the corresponding $M_{\rm gas}M_*$ "main sequence." In their work, this main sequence is constructed as the median value of $\log M_{\rm gas}$ in bins of $\log M_*$ for star-forming galaxies (SFGs); similarly, $\Delta\Sigma_1$ is defined as the deviation from the median Σ_1 in bins of M_* for SFGs. Our results reproduce the general trends of their Figure 11, although we find a steeper correlation between H₂ content and $\Delta\Sigma_1$ than reported by Ma et al. (2022). While $f_{\rm H2}$ declines by ~ 1 dex between $\Delta \Sigma_1 \approx -0.2$ and 0.2 dex in our sample, Ma et al. (2022) find that $\log M_{\rm H_2MS}$ decreases by only ~ 0.25 dex in this same range in $\Delta\Sigma_1$. We also observe a flatter trend between HI gas fraction and $\Delta\Sigma_1$ than they report. We attribute these discrepancies partly to our different definition of $\Delta\Sigma_1$ and, to our choice of using cold gas fractions (i.e., $M_{\rm H_2}/M_*$) rather than a cold gas main sequence. Our primary goal is to assess $\Delta\Sigma_1$ as an indicator of quenching, so employing the definition from Luo et al. (2020) – which is independent of any star-forming or quenched designation - offers a potentially less biased parameterization for tracking the depletion of cold gas during quenching. Regardless of the technical differences, our work provides observational evidence supporting the conclusion of Ma et al. (2022).

To summarize, our results in Figure 6 suggest that the growth of the inner stellar mass surface density at fixed mass is more closely linked to a depletion in $\rm H_2$ gas content rather than HI content, as indicated by the greater decrease in gas fraction in the vicinity of $\Delta \Sigma_1 = 0$. This trend is also coincident with a decrease in sSFR. The primary implication of this trend, if interpreted as an evolutionary one, is that massive galaxy quenching is accompanied predominantly by the removal or depletion of molecular gas rather than atomic gas as the central bulge grows.

However, we cannot rule out the possibility that the apparent differences in how $f_{\rm HI}$ and $f_{\rm H2}$ depend on $\Delta\Sigma_1$ are merely byproducts of other correlations – namely the bimodal relationship between $\Delta\Sigma_1$ and sSFR, and the different dependencies of molecular and atomic gas

fractions on sSFR. In particular, $f_{\rm H2}$ correlates more strongly with sSFR than does $f_{\rm HI}$ (e.g. Saintonge & Catinella 2022). Moreover, because $\rm H_2$ is typically more concentrated in galaxy centers, the differing trends observed between $f_{\rm HI}$ and $f_{\rm H2}$ with $\Delta\Sigma_1$ could simply reflect quenching mechanisms associated with central bulge growth and with the resulting reduction in global sSFR, rather than physical differences in HI vs. $\rm H_2$ gas depletion. In any case, our results support that the interplay of these three parameters is important for the quenching of massive galaxies at fixed mass.

4.3. The Connection to AGN Activity

As seen in Figure 7, we observe a fairly significant decrease in $f_{\rm H2}$ and a complementary increase in the number of AGN host candidates – both Seyfert and LINER – across $\Delta\Sigma_1 = 0$. Superficially, this fits into the picture of inside-out quenching, possibly aided by AGN feedback. Combined with the fact that H₂ gas is concentrated more in the centers of galaxies than HI gas, our findings are suggestive of a model by which the gas available for star formation is either expelled predominantly from the inner regions of the galaxy, or prevented from cooling or accumulating further near the galactic center by some other means; gas in the outskirts of the galaxy is not as affected. The coincident rise of potential AGN activity, gas depletion and central bulge growth could suggest that AGN feedback is at least in part responsible for the decrease of cold gas in the center regions of galaxies, but we cannot ascertain this causation from the nature of our analysis. At minimum, our results show that AGN activity is associated with lower cold gas fractions.

Nonetheless, we can postulate as to the relevance and modes of AGN feedback in our sample from an investigation of trends in Seyfert and LINER abundances with gas fraction and $\Delta\Sigma_1$. It is interesting to note that some of the greatest changes in observable properties – including Seyfert and LINER abundances – in our sample occur between $\Delta\Sigma_1 \approx 0$ dex and 0.2 dex (Figures 6 and 7). If galaxies begin to cross the green valley at $\Delta\Sigma_1 = 0$, marking the point at which galaxies begin to quench, then it would seem that most galaxies (> 70%) are quenched by $\Delta\Sigma_1 \approx 0.2$ dex and mostly depleted in molecular and atomic gas (Figure 6).

The greatest abundance of Seyfert candidates relative to the overall population occurs near $\Delta \Sigma_1 \approx 0.2$ dex (Figure 7). It is well known that Seyfert nuclei tend to be hosted by bulge-dominated, early-type spiral galaxies (e.g. Moles et al. 1995), so it is unsurprising that Seyfert hosts tend to have elevated $\Delta \Sigma_1$. However, while there is sufficient evidence for the effects of Seyfert AGN feed-

back on the innermost regions of galaxies, studies of the global cold gas contents of local Seyfert host galaxies have yielded mixed results. High-mass Seyfert hosts may not exhibit differences in their galactic-scale $\rm H_2$ fractions compared to SFGs of the same mass (Salvestrini et al. 2022), and HI observations of Seyfert hosts suggest that some may actually be enriched in their HI gas fractions (e.g. Hunt et al. 1999). In Figure 7, we find that Seyfert hosts exhibit a range of HI and $\rm H_2$ gas fractions, reflecting the complex relationship between Seyfert nuclei and the gas reservoirs of their host galaxies. It is also challenging to infer the influence of Seyfert AGN feedback on population-level trends, since only 20% of the population at $\log \Delta \Sigma_1 \approx 0.2$ dex is categorized as being in a Seyfert phase (Figure 7).

It is well known that there is a greater abundance of LINERs in the nearby Universe, which is reflected in our Figure 7. While LINER-like emission may trace older stellar populations rather than AGN activity (e.g. Singh et al. 2013), still other studies contend that many LINERs in the nearby Universe do represent genuine, low-luminosity AGN, possibly even fueling outflows (e.g. Márquez et al. 2017). Regardless of the source of the emission, some LINERs may be responsible for maintaining quiescence in nearby galaxies via "maintenance mode feedback", as evidenced by kinematic disturbances in ionized gas (e.g. Gatto et al. 2024). The galaxies in our sample with LINER-like emission-line flux ratios are predominantly quenched, gas-poor systems. While approximately 90% of these galaxies have $EW_{H\alpha} < 3$ Å, which is consistent with photoionization by older stars, this does not rule out the possibility that many of these galaxies were once powered by AGN and are now retired.

We additionally consider if our BPT classification could have missed obscured AGN in the star-forming and composite regions of the diagram. Although it is possible for AGN to be obscured by dust on galactic scales (Hickox & Alexander 2018), our sample selection minimizes this concern. The Luo et al. (2020) catalog excludes edge-on systems, mitigating the impact of dust attenuation in the host galaxy that can suppress optical AGN signatures (Hickox & Alexander 2018). Obscured AGN are also more commonly associated with gas-rich mergers, where inflows can fuel both star formation and nuclear activity behind substantial columns of dust (Hopkins et al. 2008). To confirm that our sample does not include mergers, we cross-matched our sample with Galaxy Zoo classifications (Lintott et al. 2011; Willett et al. 2013) and found no objects explicitly defined as a merger. Given the absence of mergers and our selection against edge-on geometries, it is unlikely that we are missing a population of heavily obscured AGN.

Our result that fixed-mass central bulge growth is connected to possible AGN activity and molecular gas depletion, rather than atomic gas depletion, is consistent with other studies of the impact of AGN feedback on massive galaxies in the nearby Universe. It has been suggested that AGN feedback is not likely a primary cause of global HI depletion in nearby galaxies (Fabello et al. 2011; Geréb et al. 2015). There is evidence for galactic-scale outflows of molecular gas driven by AGN feedback (e.g. Cicone et al. 2014), and Fluetsch et al. (2021) observed that for a small sample of local, ultraluminous infrared galaxies, a higher fraction of AGN-driven outflows consist of molecular rather than neutral atomic gas.

We now return to the discussion of scatter in Figures 6 and 7. While our data suggests that AGN activity and bulge growth are closely related to massive central galaxy quenching, there may be other potential quenching mechanisms at play. $\Delta\Sigma_1$ can only provide direct information about the innermost region of the galaxy, and so the role of halo or environmental effects are not captured in our work. Accounting for halo or environment properties would illuminate other possible quenching mechanisms and could potentially explain the observed variability in the $\Delta\Sigma_1 - f_{\rm H2}$ plane beyond measurement uncertainties. In addition to gas removal from the disk, recent accretion events could also contribute to the variation.

Our sample was predominantly limited to galaxies with stellar masses $M_* > 10^{10} M_{\odot}$. Future work may test the relationship between $\Delta \Sigma_1$ and cold gas fraction at stellar masses down to $M_* \sim 10^9 M_{\odot}$ to encapsulate the full range of main-sequence galaxies, which are generally supposed to quench in an inside-out fashion.

Additionally, with integral field spectroscopy (IFS), it is possible to compare the $\Delta\Sigma_1$ values for a galaxy with the distribution and kinematics of its gas reservoir. Such an analysis could offer insight into the mechanisms through which the growth of Σ_1 produces changes to the surrounding gas reservoir. There is evidence for centrally suppressed sSFR for galaxies just below the starforming main sequence (Tacchella et al. 2018). Recent IFS studies with the Atacama Large Millimeter Array have supplemented previous spatially resolved studies with sub-kpc evidence for the imprint of AGN activity on molecular gas reservoirs (e.g. Garca-Burillo et al. 2024; Holden et al. 2024). Investigations of this nature could test the strength of $\Delta\Sigma_1$ as a more readily available tracer for quenching and AGN activity, which can be applied to large samples for statistical analyses.

We have investigated the relationship between cold gas content and Σ_1 in nearby galaxies, using observations from the xGASS and xCOLDGASS surveys. We cross-matched HI and H₂ data with Σ_1 values measured by Luo et al. (2020), resulting in a sample of 341 galaxies with HI data and 201 with H₂ data. By analyzing cold gas fractions as functions of Σ_1 and the relative parameter $\Delta\Sigma_1$, we assessed how inner galactic structure is connected to the decline in global cold gas reservoirs as galaxies evolve towards quenching. Furthermore, we explored the connection between AGN activity, $\Delta\Sigma_1$, and gas fraction, offering insight into quenching mechanisms in the local Universe. We obtained the following results:

- We find comparable correlations between both the HI and H₂ cold gas fractions and Σ_1 in nearby galaxies in the regime $\Sigma_1 \gtrsim 10^9 \ M_{\odot} \ \rm kpc^{-2}$. These trends are similar in strength to previously established relationships between cold gas fractions vs. M_* and μ_* (e.g. Saintonge & Catinella 2022).
- The trend between $f_{\rm H2}$ and $\Delta\Sigma_1$ is essentially flat for galaxies below $\Delta\Sigma_1\approx 0$ then steepens above $\Delta\Sigma_1\approx 0$. This "elbow" shape is not seen in the HI gas fraction, which suggests a more direct link between molecular gas depletion and mass buildup in the bulge.
- We observe two different regimes in the plane of $f_{\rm H2}$ vs. $\Delta\Sigma_1$. Galaxies with $\Delta\Sigma_1<0$ dex tend to be gas-rich and star-forming, while those with $\Delta\Sigma_1>0$ dex tend to be gas-poor and quenched. We observe a steep decline in $f_{\rm H2}$ between $\Delta\Sigma_1\approx0$ and 0.2 dex. This threshold region marks the transition to quiescence and is accompanied by a substantial rise in AGN candidates. We propose that galaxies may evolve across this plane, undergoing a decline in their molecular gas fractions as their central bulges grow, on a path consistent with inside-out quenching and a decrease in global sSFR.
- We observe a greater abundance of AGN host candidates for $\Delta\Sigma_1 > 0$. This is consistent with the connection between AGN activity and central bulge growth, as well as the possible role of AGN feedback in gas depletion and quenching. For $\Delta\Sigma_1 \gtrsim 0.2$ dex, more than 70% of galaxies are quenched, over 60% of galaxies are AGN host candidates, and the downturn in both the HI and H₂ gas fractions levels off.

 Our findings support an inside-out quenching model in which molecular gas is preferentially depleted from the central regions of galaxies, or prevented from accumulating further, as the bulge grows, with atomic gas reservoirs being less directly impacted at fixed galaxy mass.

Prior research has shown that AGN hosts, including Seyferts and LINERs, often exhibit central deficits in molecular gas and signs of turbulence or outflows that can suppress star formation. However, while our data suggest an association between elevated $\Delta\Sigma_1$, reduced $f_{\rm H2}$, and increased AGN activity, the evidence does not confirm a direct causal relationship. Future work may involve detailed analyses of galaxies classified as Seyfert or LINER candidates that have both $f_{\rm HI}$ and $f_{\rm H2}$ measurements. This would allow us to probe whether these AGN candidates actively drive gas depletion or simply arise in already gas-poor systems. Additionally, measuring gas outflow rates can help determine whether AGN are capable of removing gas at levels sufficient to halt star formation.

This work underscores the utility of Σ_1 and $\Delta\Sigma_1$ as observational tools for tracing galaxy evolution and quenching. As larger samples and higher-resolution gas data become available, leveraging these structural parameters can help untangle the complex interplay between central bulge growth, gas depletion, and feedback mechanisms in the life-cycle of galaxies.

E. E. Shread and T. J. Weiss contributed equally to this manuscript and may both refer to this as a first-author publication. This work was funded by the Orange Coast College Foundation. We thank the anonymous referee for their insightful comments that improved this manuscript. We thank Sandra Faber for her advice on data analysis and future steps, Renata Cioczek-Georges for her insight on statistical analysis of the data, and Jessica Asbell, Yicheng Guo, and Matt Malkan for their helpful comments and insights. Thanks to Paulo Barchi, Reinaldo de Carvalho, Igor Kolesnikov, and the Cy-Morph team for sharing their morphological data during the early stages of this work.

Software: SciPy (Virtanen et al. 2020), astropy (Astropy Collaboration et al. 2013, 2018, 2022), pandas (pandas development team 2020), Matplotlib (Hunter 2007), seaborn (Waskom 2021), numpy (Harris et al. 2020), lifelines (Davidson-Pilon 2024)

Facilities: Arecibo, GALEX, WISE, IRAM-30m, APEX, SDSS, APO:2.5m

REFERENCES

- Abazajian, K. N., Adelman-McCarthy, J. K., Agueros, M. A., et al. 2009, ApJS, 182, 543, doi: 10.1088/0067-0049/182/2/543
- Astropy Collaboration, Robitaille, T. P., Tollerud, E. J., et al. 2013, A&A, 558, A33, doi: 10.1051/0004-6361/201322068
- Astropy Collaboration, Price-Whelan, A. M., Sipőcz, B. M., et al. 2018, AJ, 156, 123, doi: 10.3847/1538-3881/aabc4f
- Astropy Collaboration, Price-Whelan, A. M., Lim, P. L., et al. 2022, ApJ, 935, 167, doi: 10.3847/1538-4357/ac7c74
- Baker, W. M., Maiolino, R., Bluck, A. F. L., et al. 2021, MNRAS, 510, 3622, doi: 10.1093/mnras/stab3672
- Baldwin, J. A., Phillips, M. M., & Terlevich, R. 1981, PASP, 93, 5, doi: 10.1086/130766
- Barro, G., Faber, S., Koo, D. C., et al. 2017, ApJ, 840, 47, doi: 10.3847/1538-4357/aa6b05
- Barro, G., Faber, S. M., Pérez-González, P. G., et al. 2013, ApJ, 765, 104, doi: 10.1088/0004-637X/765/2/104
- Bentz, M. C., Denney, K. D., Grier, C. J., et al. 2013, ApJ, 767, 149, doi: 10.1088/0004-637X/767/2/149
- Bigiel, F., Leroy, A., Walter, F., et al. 2008, AJ, 136, 2846, doi: 10.1088/0004-6256/136/6/2846
- Boselli, A., Cortese, L., Boquien, M., et al. 2014, A&A, 564, A66, doi: 10.1051/0004-6361/201322312
- Brinchmann, J., Charlot, S., White, S., et al. 2004, MNRAS, 351, 1151, doi: 10.1111/j.1365-2966.2004.07881.x
- Drawn T. Catinalla D. Cartaga I. at a
- Brown, T., Catinella, B., Cortese, L., et al. 2015, MNRAS, 452, 24792489, doi: 10.1093/mnras/stv1311
- Catinella, B., Saintonge, A., Janowiecki, S., et al. 2018, MNRAS, 476, 875, doi: 10.1093/mnras/sty089
- Catinella, B., Schiminovich, D., Kauffmann, G., et al. 2010, MNRAS, 403, 683, doi: 10.1111/j.1365-2966.2009.16180.x
- Catinella, B., Schiminovich, D., Cortese, L., et al. 2013, MNRAS, 436, 34, doi: 10.1093/mnras/stt1417
- Cheung, E., Faber, S., Koo, D. C., et al. 2012, ApJS, 760, 131, doi: 10.1088/0004-637X/760/2/131
- Cicone, C., Maiolino, R., Sturm, E., et al. 2014, A&A, 562, A21, doi: 10.1051/0004-6361/201322464
- Cid Fernandes, R., Stasiska, G., Mateus, A., & Vale Asari, N. 2011, MNRAS, 413, 1687, doi: 10.1111/j.1365-2966.2011.18244.x
- Conselice, C. J. 2014, ARAA, 476, 875, doi: 10.1146/annurev-astro-081913-040037
- Croton, D. J., Springel, V., White, S. D. M., et al. 2006, MNRAS, 365, 1128, doi: 10.1111/j.1365-2966.2005.09675.x
- Davidson-Pilon, C. 2024, lifelines, survival analysis in Python, v0.30.0, Zenodo, doi: 10.5281/zenodo.14007206

- Davis, T. A., Gensior, J., Bureau, M., et al. 2022, MNRAS, 512, 1522, doi: 10.1093/mnras/stac600
- Dubois, Y., Gavazzi, R., Peirani, S., & Silk, J. 2013, MNRAS, 433, 3297, doi: 10.1093/mnras/stt997
- Fabello, S., Kauffmann, G., Catinella, B., et al. 2011, MNRAS, 416, 1739,
 - doi: 10.1111/j.1365-2966.2011.18825.x
- Fang, J. J., Faber, S., Koo, D. C., et al. 2013, ApJ, 776, 63, doi: 10.1088/0004-637X/776/1/63
- Feigelson, E. D., & Nelson, P. I. 1985, ApJ, 293, 192
- Fernandes, R. C., Stasiska, G., Schlickmann, M. S., et al. 2010, MNRAS, 403, 1036,
 - doi: 10.1111/j.1365-2966.2009.16185.x
- Fisher, D. B., Bolatto, A., Drory, N., et al. 2013, ApJ, 764, 174, doi: 10.1088/0004-637X/764/2/174
- Fluetsch, A., Maiolino, R., Carniani, S., et al. 2021, MNRAS, 505, 5753, doi: 10.1093/mnras/stab1666
- Garca-Burillo, S., Hicks, E. K. S., Alonso-Herrero, A., et al. 2024, A&A, 689, A347, doi: 10.1051/0004-6361/202450268
- Gatto, L., Storchi-Bergmann, T., Riffel, R. A., et al. 2024, MNRAS, 530, 3059, doi: 10.1093/mnras/stae989
- Geréb, K., Morganti, R., Oosterloo, T. A., Hoppmann, L., & Staveley-Smith, L. 2015, A&A, 580, A43, doi: 10.1051/0004-6361/201424810
- Guo, Y., Carleton, T., Bell, E. F., et al. 2021, ApJ, 914, 7, doi: 10.3847/1538-4357/abf115
- Hagedorn, B., Cicone, C., Sarzi, M., et al. 2024, A&A, 687, A244, doi: 10.1051/0004-6361/202449773
- Harris, C. R., Millman, K. J., van der Walt, S. J., et al. 2020, Nature, 585, 357, doi: 10.1038/s41586-020-2649-2
- Hickox, R. C., & Alexander, D. M. 2018, ARAA, 56, 625, doi: 10.1146/annurev-astro-081817-051803
- Holden, L. R., Tadhunter, C., Audibert, A., et al. 2024, MNRAS, 530, 446, doi: 10.1093/mnras/stae810
- Hopkins, P. F., Hernquist, L., Cox, T. J., & Kere, D. 2008, ApJS, 175, 356, doi: 10.1086/524362
- Huang, S., Haynes, M. P., Giovanelli, R., et al. 2012, ApJ, 756, 113, doi: 10.1088/0004-637X/756/2/113
- Hunt, L. K., Malkan, M. A., Moriondo, G., & Salvati, M. 1999, ApJ, 510, 637, doi: 10.1086/306607
- Hunt, L. K., Tortora, C., Ginolfi, M., et al. 2020, AAP, 643, A180, doi: 10.1051/0004-6361/202039021
- Hunter, J. D. 2007, Computing in Science & Engineering, 9, 90, doi: 10.1109/MCSE.2007.55
- Kauffmann, G., Li, C., Fu, J., et al. 2012, MNRAS, 442, 997, doi: 10.1111/j.1365-2966.2012.20672.x

- Kauffmann, G., Heckman, T. M., Tremonti, C., et al. 2003, MNRAS, 346, 1055,
 - doi: 10.1111/j.1365-2966.2003.07154.x
- Kelly, B. C. 2007, ApJ, 665, 1489, doi: 10.1086/519947
- Kewley, L. J., Dopita, M. A., Sutherland, R. S., Heisler,C. A., & Trevena, J. 2001, ApJ, 556, 121,doi: 10.1086/321545
- Khan, F. M., Rodrguez, ., Macci, A. V., Sharma, S., & Cho, C. 2025, ApJ, 990, 6, doi: 10.3847/1538-4357/ade99e
- Kumari, N., Maiolino, R., Trussler, J., et al. 2021, A&A, 656, A140, doi: 10.1051/0004-6361/202140757
- Lee, B., Giavalisco, M., Whitaker, K., et al. 2018, ApJ, 853, 131, doi: 10.3847/1538-4357/aaa40f
- Leroy, A. K., Walter, F., Brinks, E., et al. 2008, AJ, 136, 2782, doi: 10.1088/0004-6256/136/6/2782
- Lin, L., Faber, S., Koo, D. C., et al. 2020, ApJ, 899, 93, doi: 10.3847/1538-4357/aba755
- Lintott, C. J., Schawinski, K., Bamford, S., et al. 2011, MNRAS, 410, 166, doi: 10.1111/j.1365-2966.2010.17432.x
- Luo, Y., Faber, S., Rodriguez-Puebla, A., et al. 2020, MNRAS, 493, 1686, doi: 10.1093/mnras/staa328
- Ma, W., Liu, K., Guo, H., et al. 2022, ApJ, 941, 205, doi: 10.3847/1538-4357/aca326
- Márquez, I., Masegosa, J., González-Martin, O., et al. 2017, FSPAS, 4, doi: $10.3389/\mathrm{fspas}.2017.00034$
- McConnell, N. J., & Ma, C.-P. 2013, ApJ, 764, 184, doi: 10.1088/0004-637X/764/2/184
- Moles, M., Márquez, I., & Pérez, E. 1995, ApJ, 438, 604
- Namiki, S. V., Koyama, Y., Koyama, S., et al. 2021, ApJ, 918, 68, doi: 10.3847/1538-4357/abfe08
- pandas development team, T. 2020, pandas-dev/pandas: Pandas, latest, Zenodo, doi: 10.5281/zenodo.3509134
- Piotrowska, J. M., Bluck, A. F. L., Maiolino, R., & Peng, Y. 2021, MNRAS, 512, 1052, doi: 10.1093/mnras/stab3673
- Popping, G., Behroozi, P. S., & Peeples, M. S. 2015, MNRAS, 449, 477, doi: 10.1093/mnras/stv318
- Roberts, M. S. 1969, AJ, 74, 859, doi: 10.1086/110874
- Roberts, M. S., & Haynes, M. B. 1994, ARAA, 32, 115, doi: 10.1146/annurev.aa.32.090194.000555
- Sage, L. J. 1993, A&A, 100, 537
- Saintonge, A., & Catinella, B. 2022, ARAA, 60, 319, doi: 10.1146/annurev-astro-021022-043545

- Saintonge, A., Catinella, B., Tacconi, L. J., et al. 2017, ApJS, 233, 22, doi: 10.3847/1538-4365/aa97e0
- Saintonge, A., Kauffmann, G., Kramer, C., et al. 2011, MNRAS, 415, 32, doi: 10.1111/j.1365-2966.2011.18677.x
- Salvestrini, F., Gruppioni, C., Hatziminaoglou, E., et al. 2022, A&A, 663, A28, doi: 10.1051/0004-6361/202142760
- Sancisi, R., Fraternali, F., Oosterloo, T., & van der Hulst,
 T. 2008, A&ARv, 15, 189,
 doi: 10.1007/s00159-008-0010-0
- Singh, R., van de Ven, G., Jahnke, K., et al. 2013, A&A, 558, A43, doi: 10.1051/0004-6361/201322062
- Su, K.-Y., Hopkins, P. F., Hayward, C. C., et al. 2019, MNRAS, 487, 43934408, doi: 10.1093/mnras/stz1494
- Tacchella, S., Carollo, C. M., Schreiber, N. M. F., et al. 2018, ApJ, 859, 56, doi: 10.3847/1538-4357/aabf8b
- van Dokkum, P. G., Nelson, E. J., Franx, M., et al. 2015, ApJ, 813, 23, doi: 10.1088/0004-637X/813/1/23
- Virtanen, P. T., Gommers, R., Oliphant, T. E., et al. 2020, Nature Methods, 17, 261, doi: 10.1038/s41592-019-0686-2
- Wang, J., Kauffmann, G., Overzier, R., et al. 2011, MNRAS, 412, 1081,
 - doi: 10.1111/j.1365-2966.2010.17962.x
- Waskom, M. L. 2021, Journal of Open Source Software, 6, 3021, doi: 10.21105/joss.03021
- Willett, K. W., Lintott, C. J., Bamford, S. P., et al. 2013, MNRAS, 435, 2835, doi: 10.1093/mnras/stt1458
- Woo, J., Carollo, C. M., Faber, S. M., Dekel, A., & Tacchella, S. 2016, MNRAS, 464, 1077, doi: 10.1093/mnras/stw2403
- Woo, J., Faber, S., Dekel, A., et al. 2015, MNRAS, 448, 237, doi: 10.1093/mnras/stu2755
- Yesuf, H. M., & Ho, L. C. 2019, ApJ, 884, 177, doi: 10.3847/1538-4357/ab4202
- Young, J. S., & Knezek, P. M. 1989, ApJ, 347, L55, doi: 10.1086/185606
- Young, J. S., & Scoville, N. Z. 1991, ARAA, 29, 581, doi: 10.1146/annurev.aa.29.090191.003053
- Zhang, C., Peng, Y., Ho, L. C., et al. 2019, ApJL, 884, L52, doi: 10.3847/2041-8213/ab4ae4
- Zhou, Z., Wu, H., Zhou, X., et al. 2018, PASP, 130, 1, doi: 10.1088/1538-3873/aad407